Meccanica (2022) 57:2863–2883
https://doi.org/10.1007/s11012-022-01603-8

Similarities in steering control between cars and motorcycles: application to a low-complexity riding simulator

Mirco Bartolozzi · Lorenzo Berzi · Enrico Meli · Giovanni Savino

Received: 20 July 2022 / Accepted: 16 October 2022 / Published online: 25 October 2022

Abstract Motorcycle simulators are employed for rider training, studying human–machine interaction, and developing assistance systems. However, existing simulators are either too simple and, therefore, unsuitable or significantly complex, with higher hardware costs and familiarisation times. This study aimed to use a tuned single-track car model as the basis of a motorcycle simulator, leading to considerable software simplification while preserving its fidelity. In particular, the approach defined a conversion between motorcycle steering torque and car steering angle. It modified the parameters of the latter to reproduce the response of various motorcycle models in quasi-static and transient conditions for different speeds and radii of curvature. A robust manoeuvrability index was chosen. For the car, it was possible to calculate it from its parameters analytically. Next, the car yaw inertia was tuned to obtain a motorcycle-like steering response. Finally, the calibrated car model was implemented into a low-complexity motorcycle simulator for objective validation. It was verified that an understeering single-track model with high yaw inertia has amplitude and phase responses analogous to a motorcycle. The experimental results of the simulator test confirmed these findings for a diverse set of manoeuvres, validating the method. This straightforward approach allows the development of low-complexity simulators with good steering fidelity, using an objective procedure to reproduce the behaviour of a chosen motorcycle class. In addition, the low computational cost of the model makes it a potential candidate for use in assistance systems.

Keywords Motorcycle simulator · Car and motorcycle manoeuvrability · Car and motorcycle dynamics · Simulation · Frequency response and transfer functions · Objective and quantitative validation

1 Introduction

Riding simulators are a fundamental tool for driver training and the development of assistance systems. However, the complexity of realistically simulating two-wheeled vehicles has meant that the development and adoption of motorcycle simulators have

Lorenzo Berzi, Enrico Meli and Giovanni Savino these authors contributed equally to this study.

M. Bartolozzi (✉) · L. Berzi · E. Meli · G. Savino
Dipartimento di Ingegneria Industriale, Università degli Studi di Firenze, Via di Santa Marta 3, 50139 Florence, Tuscany, Italy
e-mail: mirco.bartolozzi@unifi.it

L. Berzi
e-mail: lorenzo.berzi@unifi.it

E. Meli
e-mail: enrico.meli@unifi.it

G. Savino
e-mail: giovanni.savino@unifi.it

been more limited than others, such as automotive simulators.

The literature offers several examples of high-complexity simulators seeking high realism. One notable example is the DIMEG simulator [1]: the measured motorcycle commands are the control inputs of a complex, nonlinear, 14-DoF motorcycle model [2] able to reproduce the most critical motions and instabilities of such vehicle. Another input is the rider lean. The accelerations of the virtual motorcycle are converted into lateral, yaw, roll, pitch and steer motions. The hardware and software complexity of this simulator allows high physical agreement and realism [3]; however, it makes the simulator expensive and challenging to transport, with dedicated personnel for its use and maintenance.

The IFSTTAR simulator [4] is more straightforward than the DIMEG simulator but still quite complex. An active platform reproducing the most significant inertial effects of the vehicle executes the roll for the reproduction of quick cornering, the pitch, inducing the sensation of longitudinal acceleration, and yaw for the impression of instability induced by the skidding of the rear wheel. This approach significantly reduces complexity and cost. In addition to the steering degree of freedom, with the corresponding torque exerted by an electric motor, the handlebar can translate along the longitudinal axis of the mockup. This additional motion provides the sensation of longitudinal acceleration due to the inertia forces acting on the rider's chest.

Lastly, the Portable Driving Simulator [5] is a simplified version of the DIMEG simulator: the hardware is much simpler to allow transportation, with active roll motion as the only degree of freedom. The steering input consists of the steering torque applied by the rider, measured by a torque sensor; however, the steering is fixed, and the feedback torque felt by the rider is just the reaction force applied by the handlebar, equal and opposite to the steering torque applied. Even though the hardware used is much simpler, the motorcycle and tyre models still derive from those described by Cossalter [1], with just a little reduction in complexity. As demonstrated by Massaro [5], this approach still allows the description of characteristic motorcycle behaviours and vibratory modes but introduces difficulties in starting from a standstill and in low-speed manoeuvres.

A high-complexity simulator, although providing a high level of objective agreement between simulated and real vehicle dynamics, does not guarantee an optimal steering feeling. Several fidelity and validity issues affect even sophisticated simulators [6]. An initial adaptation process is required in which the user has to learn the simulator outputs to transfer their driving skills to the simulator, and it is a precondition for the validity of experiments involving the simulator [7]. In particular, Benedetto [6] compared a positive steering configuration and a counter-steering configuration on the same simulator. The second was the most demanding, with a longer adaptation process. However, after this initial period, it showed higher realism than the other and was preferred by riders. The conclusion made by the author is that counter-steering is to be preferred to positive steering at higher speeds [8]. The existing rider control models justify this: the steering controller works as a position servo at low speeds, and a torque servo at higher speeds [9].

The Honda Riding Trainer is a low-complexity training tool for novice riders. The only Degree of Freedom (DoF) allowed is the steering motion, and the leaning is reproduced only by tilting the horizon. Although not focusing on realistic steering inputs and with little perceived realism, it has been widely used for training purposes, to study hazard perception and mental workload [6].

A more straightforward simulator aiming at reproducing the correct steering feel while renouncing some of the realism in other aspects might guarantee better results in this specific aspect. One alternative solution [10] proposed a low-complexity, reproducible approach in which the front assembly is a simple rotational inertia-spring system. The steering feedback to the rider does not involve any power actuators, eliminating associated costs and tuning. The realism of the steering input is based on an empirical similitude between the dynamic behaviour of four-wheeled vehicles and tilting two-wheeled vehicles. A low-complexity simulator requires shorter familiarisation procedures [6], making it better suited for experiments with numerous participants. Moreover, its cost-effective nature allows adoption by a wider audience of subjects for training purposes, assistance system development, investigation of human–machine interaction and rider modelling.

In particular, it may allow to easily convert any car simulation facility into a motorcycle simulator with realistic steering sensation by adding a low-complexity motorcycle mockup. The simulator received favourable ratings for its realism and handling, even for the first familiarisation test, indicating a short adaptation period. Concerning the objective validation, although the measured steering inputs showed qualitative agreement with reference data, their amplitude did not match. Nugent [11] showed higher required input compared to a real motorcycle during steady corners and lower during transient manoeuvres as the lane change. The car parameters were the default ones, and the steering torque applied to the handlebar was converted to a car steering angle through a gain. The gain was subjectively chosen to allow a good compromise between the torque required during steady and transient manoeuvres, but the default car parameters prevented an optimal description of both.

Such a low-complexity motorcycle riding simulator offers a reproducible, clear and unambiguous platform. The two gaps we focus on are a more careful evaluation of the similarities and differences in manoeuvrability between a car and a motorcycle and correct calibration of the model's parameters that allow stationary and transient manoeuvres reproduction. A simplified simulator must be correctly calibrated in order to exploit its virtues. For simulators of this type in the literature, this is done subjectively with a trial-and-error approach. An objective, reproducible method capable of emulating the response of different motorcycle classes would facilitate the realisation of such simulators.

The remainder of the paper is organised as follows: the vehicle models considered in this study are introduced and described in Sect. 2; then, Sect. 3 investigates the similarities between the motorcycle and car manoeuvrability, first in quasi-static conditions and then during transient manoeuvres, and defines the calibration procedure used to obtain the equivalence. Section 4 describes the simulator and testing procedure used for the experimental validation; results are shown and discussed in Sect. 5. Lastly, Sect. 6 discusses and sums up the results and their implications, accompanied by potential improvements and applications of the approach.

2 Vehicle models

Our work focuses on the similarities and differences between the dynamics of low-complexity versus high-fidelity models and between motorcycle and car models.

2.1 High-fidelity and simplified motorcycle models

Complex motorcycle models accurately describe general and detailed phenomena that constitute motorcycle dynamics. For example, the high-fidelity model used as the basis of the DIMEG simulator is described by Cossalter [2]. In the case of telescopic front forks and rear swingarm, the model consists of the main body (including the rear-end and the rider's lower body), the swingarm, the rider's upper body, the two wheels and the steering assembly, which can rotate and translate along its axis and twist perpendicularly to it. The model includes the features that significantly influence motorcycle dynamics and is an evolution of the one described by Cossalter and Lot [12].

In this work, the commercial software BikeSim© (Mechanical Simulations, Ann Arbor, MI, US) [13] simulated the high-fidelity motorcycle dynamics. Its model is based on that developed and validated by Sharp [14, 15]. Compared to that, it adds, for example, an entire powertrain, nonlinear suspension and additional degrees of freedom. The rider's lower body is now separate from the motorcycle's main body, with relative translational and rotational motion. The optional TNO MF-Swift tyre model [16] can describe tyre behaviour up to 100 Hz. The model includes feedforward PID controllers for path tracking and speed-profile following. The rider's body motion can either be passive (i.e. determined by the stiffness-damping-inertia properties of its upper and lower body and the inertial forces acting on it) or active (with movement based on a previously defined logic).

High-fidelity motorcycle models are ideal for conducting dynamics simulations, as long as it is possible to identify the numerous parameters of the motorcycle of interest or if default values are available to the user for different motorcycle classes, like in BikeSim©. However, when used as the basis of a simulator, they lead to additional complexity [6]. An alternative could be using a simplified motorcycle model, like the first model proposed by Sharp [17]:

this model is nonlinear, but its equations can be linearised considering small perturbations from straight running. Tyre forces are a linear combination of tyre slip and camber, including a relaxation behaviour; tyre moments due to turnslip and pneumatic trail are neglected. Tyres are lenticular, leading to lower roll angle values than toroidal wheels [18] unless an overturning moment is included separately [19]. This aspect influences the simulation because the lower roll angle causes lower camber angles and, thus, lower camber thrust, so the slip angles have to change to maintain equilibrium. The rider may not perceive this effect but would likely notice the missing brake steering torque following front wheel braking. Moreover, the yawing moments due to the turnslip and the pneumatic trail greatly influence the steering torque, as does the lateral displacement of the contact patch due to the tyre being toroidal [20]: neglecting these contributions leads to a significant error on the steering torque computation even when the other parameters have correct values, thus potentially reducing the simulator fidelity.

Additionally, a simplified motorcycle model would still cause problems due to the motorcycle's unstable nature (at low speed) and the rider's inability to stabilise the motorcycle while riding the simulator using all the inputs (e.g. body movement) available in reality. In particular, starting from and braking to a standstill would lead to a fall unless the dynamics are significantly modified under a certain speed threshold. Due to limited benefits and significant additional problems, we discarded the simplified motorcycle model as the dynamic model of the simulator in favour of a simplified car model, as employed previously [10], described in the following subsection.

2.2 Linearised single-track car model

A single-track model approximates car dynamics: in this representation, the left and right wheels of the same axis are lumped together, and suspension kinematics is neglected. Single-track models can have varying levels of complexity [21] and are helpful for state estimation [22] and for describing the essential dynamics of a car [23]. Instead, a complete model is preferred to simulate manoeuvres which are more demanding concerning acceleration and frequency [24].

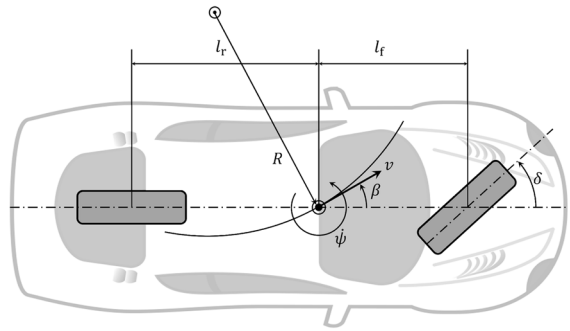

Fig. 1 Scheme of the single-track model

The simplest single-track car model is the linearised, two-degree-of-freedom model: it is valid under the small-angle assumption and considers linear tyre behaviour. Figure 1 depicts the scheme for the model used in this work: it considers dynamic steering and not kinematic steering, as is evident from the centre of instantaneous rotation not lying on the rear axle extension.

Its state-space representation uses the vehicle's slip angle β and its yaw rate $r = \dot{\psi}$ as the two states:

$$\begin{pmatrix} \dot{\beta} \\ \dot{r} \end{pmatrix} = \begin{bmatrix} -\frac{C_f+C_r}{mv} & \frac{l_rC_r-l_fC_f}{mv^2} - 1 \\ \frac{l_rC_r-l_fC_f}{I_z} & -\frac{l_f^2C_f+l_r^2C_r}{I_zv} \end{bmatrix} \begin{pmatrix} \beta \\ r \end{pmatrix} + \begin{bmatrix} \frac{C_f}{mv} \\ \frac{l_fC_f}{I_z} \end{bmatrix} \delta. \tag{1}$$

The vehicle's parameters are as follows: m is vehicle's mass; I_z is its yaw, barycentric inertia; l is the wheelbase, divided by the centre of mass into its front and rear portions $l_{f,r}$; $C_{f,r}$ are the front and rear cornering stiffnesses. v is the vehicle's speed, which is a parameter in case of uncombined lateral dynamics. From the perspective of dynamical systems theory, the only input is the kinematic steering angle δ.

Equation (1) can be rewritten in the compact form:

$$\dot{\boldsymbol{x}} = \mathrm{A}\boldsymbol{x} + \boldsymbol{b}\delta. \tag{2}$$

The state vector $\boldsymbol{x}$, comprising the vehicle's slip angle β and its yaw rate r, changes due to free evolution from the initial states and to the steering input. When considering the steady-state behaviour, $\dot{\boldsymbol{x}} = 0$ holds, and Eq. (2) becomes a system of two algebraic equations. In that case, both δ and v can be interpreted

as inputs, with β and r as the corresponding outputs, obtained by solving the algebraic system.

Using this simple, readily available and computationally-efficient model for motorcycle riding simulation requires proving the similarity between this car model and a general motorcycle model; then, its parameters must be adapted to make it behave as a reference motorcycle.

3 Similarities between motorcycle and car manoeuvrability

The perceived simulator realism is linked to the input–output relationship underlying the simulator dynamics: simpler simulators can have a high perceived realism as long as the primary input–output relationships are correctly reproduced [6]. In our case, the input–output relationship is from the applied steering input (steering torque) to the lateral response of the vehicle (lateral motion, in terms of yaw rate or lateral acceleration). We aim to accurately describe this relationship based on the behaviour of a reference, high-fidelity motorcycle model while using a linear single-track car model as the dynamic model of the simulator. In order to do so, a similarity between the steering response of the two vehicles must be identified. In other words, the two vehicles must have similar manoeuvrability [25]. This section investigates this aspect.

3.1 Quasi-static conditions

Let us analyse manoeuvrability in quasi-static conditions. Similar behaviour is obtained in an overlap region, showing a correspondence between car and motorcycle control inputs. Triads comprising the forward vehicle speed, the radius of curvature of the trajectory and the steering input, subsequently referred to as *quasi-static curve maps*, are compared.

The triads for the high-fidelity motorcycle model were obtained through BikeSim© simulation. The Touring, Scooter, and Sports Small models were considered, having different parameters representing different motorcycle classes. Details about the exact procedure are provided in Appendix A.

The triads for the simplified car model are based on the dynamics described by Eq. (1). For stationary or quasi-static manoeuvres, the dynamic term can be neglected ($\dot{\boldsymbol{x}} = 0$). The system can be solved for δ obtaining:

$$\delta = \frac{l\left(1 + \eta v^2\right) r}{v}, \tag{3}$$

where η is the *understeer coefficient* that depends solely on car parameters:

$$\eta = \frac{m}{l^2}\left(\frac{l_\mathrm{r} C_\mathrm{r} - l_\mathrm{f} C_\mathrm{f}}{C_\mathrm{f} C_\mathrm{r}}\right). \tag{4}$$

In particular, it depends on all car parameters except the yaw inertia I_z. Lastly, we substitute $v = Rr$ into Eq. (3), obtaining:

$$\delta = \frac{l\left(1 + \eta v^2\right)}{R}. \tag{5}$$

We can use this equation to calculate the steering angle δ required to complete a curve of radius R at a given speed v for a specific set of car parameters. In particular, three front-to-rear splits of front and rear cornering stiffness $C_{\mathrm{f,r}}$ were used to have oversteering, neutral and understeering behaviour, resulting in a negative, null or positive understeer coefficient, respectively. Lastly, values where lateral acceleration $a_y = v^2/R$ exceeded the value corresponding to 40° motorcycle roll, were excluded.

Figure 2 shows the absolute value of the steering torque applied as a function of curvature radius and speed for the *Touring* (left), *Scooter* (centre) and *Sports Small* models (right). In contrast, Fig. 3 shows the absolute value of the kinematic steering angle required by the car model for the same independent variables, for the *oversteering* (left), *neutral* (centre) and *understeering* (right) vehicle. A qualitative examination of steering torques for motorcycles shows a trend with common characteristics for combinations of low speeds and high radii of curvature. In particular, there was a monotonic increase in steering torque for the same radius with increasing speed. These zones generally correspond to low and medium roll angles: at higher roll angles, the trend can reverse, as seen for the Touring motorcycle. The presence or absence and positioning of flexes at combinations such as high speeds and relatively low radii of curvature (corresponding to pronounced roll angles) distinguish the motorcycle models examined, which have qualitatively the same trend in the rest of the map.

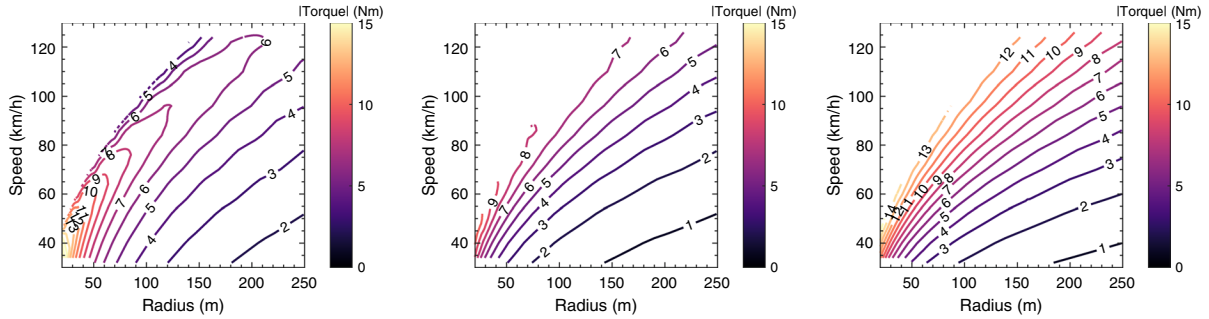

(a) Touring motorcycle **(b)** Scooter **(c)** Sports Small motorcycle

Fig. 2 *Quasi-static curve maps* for three different motorcycle models, showing the absolute value of the steering torque as a function of curve radius and speed

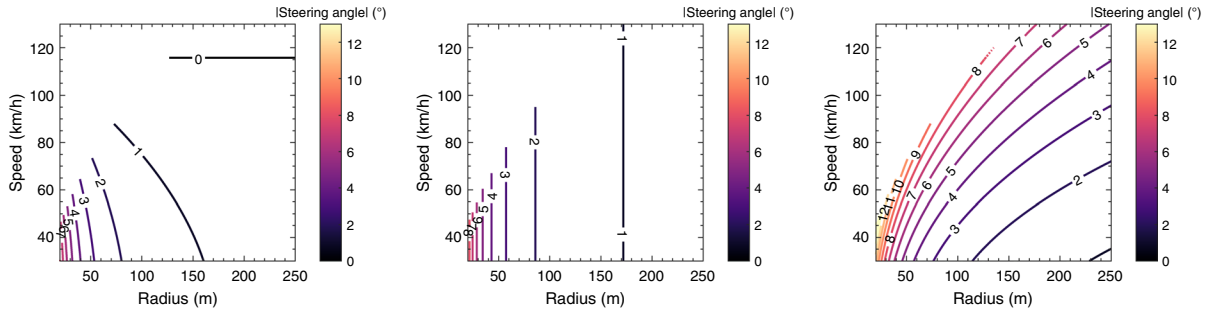

(a) Oversteering car **(b)** Neutral car **(c)** Understeering car

Fig. 3 *Quasi-static curve maps* for three sets of car parameters, showing the absolute value of the steering angle as a function of curve radius and speed

Results are coherent with ones present in the literature [20, 26].

Although the two figures have different dependent variables (torque and angle, respectively), they can be compared qualitatively. In particular, the *quasi-static curve map* of the *Sports Small* motorcycle is similar to that of the understeering car in the whole radius-speed domain: both show a monotone increase of steering input with increasing speed for a specific turning radius, and with decreasing turning radius for a specific speed. Consequently, the higher the lateral acceleration, the higher the input required. For the car model, this directly follows from the understeer coefficient definition [27]. Conversely, oversteering cars require a steering angle reduction to maintain the corner radius with increasing speed, especially for higher acceleration values. Additionally, Fig. 3a shows a speed value (called *critical speed* [27]) that results in zero steering input required to corner, making the vehicle impossible to control.[1]

We can conclude that a simplified car model can have quasi-static manoeuvrability properties similar to certain motorcycles for specific sets of its parameters. Moreover, we can extend this analogy to other motorcycle classes if we exclude very high lateral acceleration values, as shown by the similar trend of the steering torque for higher corner radii and lower speeds for the three motorcycles. We call *superposition region* the locus of the speed-radius points where steering torque (for motorcycles) and steering angle (for four-wheeled vehicles) are in good approximation proportional to each other. Notably, while the car steering angle is always towards the inside of the

[1] The critical speed is never reached for passenger cars, for which the non-linear and generally understeering behaviour prevents this phenomenon.

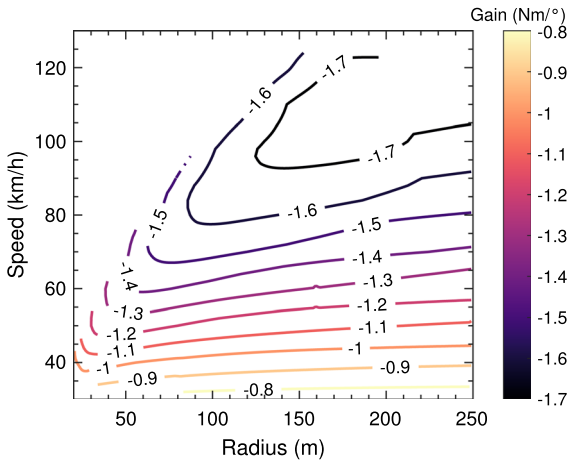

Fig. 4 Ratio of motorcycle steering torque to car steering angle, as a function of both curve radius and speed. Vehicles used: *Sports Small* motorcycle, *Understeering* car. The negative values indicate that car steering angle and motorcycle steering torque have opposite signs (due to the motorcycle counter-steering)

corner, motorcycle steering torque was (for the motorcycle models and lateral acceleration values considered) directed towards the outside of the curve.[2] This fact is due to the counter-steering action required to control a motorcycle and justifies using this approach when designing a simulator. The difference in sign between the two is not visible when comparing Figs. 2c and 3c because the maps show the absolute values of the steering input (torque or angle); otherwise, the input would change sign between left and right corners.

To make the manoeuvrability of the car model also *quantitatively* similar to that of the reference motorcycle, we can choose a reference point (R^*, v^*) and use it to calibrate the car model. We define the *equivalence gain* K_{steer} as the ratio (with sign) of motorcycle steering torque τ and car steering angle δ for the chosen reference point:

$$K_{\text{steer}} := \frac{\tau(R^*, v^*)}{\delta(R^*, v^*)}. \tag{6}$$

Its value depends on the particular reference point (R^*, v^*), as shown by Fig. 4: the graph is obtained by dividing the *Sports Small* motorcycle steering torque values (Fig. 2c) by the *Understeering* car steering angle (Fig. 3c), for the whole radius and speed domain. K_{steer} is always negative in the considered domain because the car steering angle input and the motorcycle steering torque input have opposite signs through the same corner. K_{steer} changes with speed for a certain radius, while the dependency on the radius is less pronounced. We choose a reference point (R^*, v^*) and use the equivalence gain in that point as the *calibration gain* between the steering torque applied by the rider and the steering angle imposed on the car: this way, the simplified car model corners with the same radius as the motorcycle considered, as a consequence of that specific torque applied.

Figure 5 shows the relative error obtained by comparing the quasi-static curve maps for the *Understeering* car and *Sports Small* motorcycle, assuming a calibration coefficient for $R^* = 200\,\text{m}$ and $v^* = 40\,\text{km}\,\text{h}^{-1}$ (left), $v^* = 60\,\text{km}\,\text{h}^{-1}$ (centre) and $v^* = 80\,\text{km}\,\text{h}^{-1}$ (right). The coloured area shows the region in which error $< 20\%$: for the $R^* = 200\,\text{m}$, $v^* = 80\,\text{km}\,\text{h}^{-1}$ calibration point, the error is acceptable for a vast *radius-speed* region. Moreover, a motorcycle simulator using a simplified car model is most suitable to reproduce medium to high-speed riding conditions, where the motorcycle tends to have stable modes [18] as does an understeering car, so that the real nature of the underlying model of the simulator is less noticeable (e.g. not possible to fall). In this work, the calibration gain was kept constant and, for this motorcycle model, equal to $K_{\text{steer}}|_{R^*=200\,\text{m}, v^*=80\,\text{km}\,\text{h}^{-1}} = -1.53\,\text{Nm/deg} = -87.7\,\text{N}\,\text{m}\,\text{rad}^{-1}$: the closer the simulated manoeuvre is to these conditions, the more accurate the equivalence between the simplified car behaviour and that of the reference, complex motorcycle.

The calibration gain maps and the error maps relative to the other two motorcycles are available in Appendix B and show that the error is the same or lower than that for the *Sports Small* model. In particular, the *Touring* model presents a modest error in the whole domain of interest, except for the high lateral acceleration region where Fig. 2a shows the trend reversal. Consequently, the concepts and results that, for brevity, are shown using a specific motorcycle have more general validity.

[2] We define 'torque towards the outside of the curve' a torque whose vertical component is discordant with the yaw rate of the mainframe.

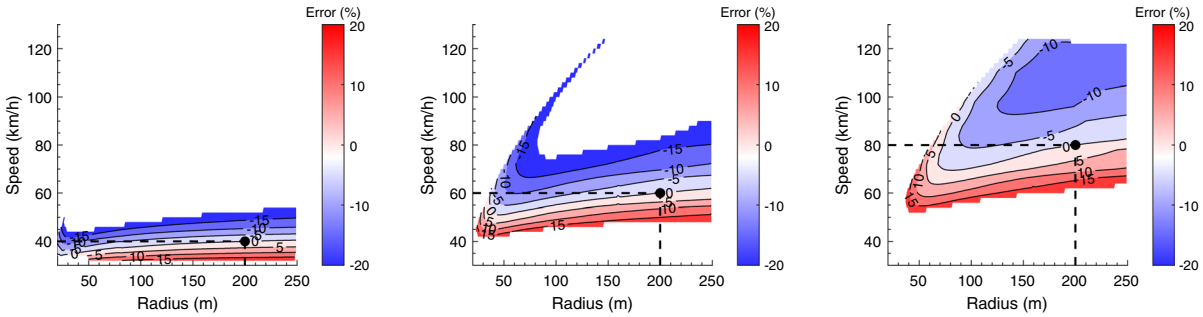

(a) $R^* = 200\,\mathrm{m},\ v^* = 40\,\mathrm{km\,h^{-1}}$ **(b)** $R^* = 200\,\mathrm{m},\ v^* = 60\,\mathrm{km\,h^{-1}}$ **(c)** $R^* = 200\,\mathrm{m},\ v^* = 80\,\mathrm{km\,h^{-1}}$

Fig. 5 Relative error using a constant *Equivalence gain* with three different calibration points. By definition, the error is zero at the calibration point. (Color figure online)

3.2 Transient conditions

The input–output relationship shown in Figs. 2, 3 is only valid for very low frequencies and does not correctly describe transient manoeuvres, such as a slalom or a lane change. When the input is varied quickly, the vehicle response is influenced, both in amplitude and phase, by the inertia and damping of the various parts and the tyre relaxation length [28], among others.

To approximate the transient motorcycle manoeuvrability through a simplified car model, we sought the equivalence of a manoeuvrability index suitable for transient manoeuvres. The *Lane Change Yaw Index* (LCYI) was chosen, defined as [29]:

$$\mathrm{LCYI}_{\mathrm{bike}} := \frac{\tau_{\mathrm{p\text{-}p}}}{\dot{\psi}_{\mathrm{p\text{-}p}} v_{\mathrm{avg}}}, \tag{7}$$

where τ is the steering torque at the handlebar, $\dot{\psi}$ is the yaw rate, and v is the speed. The subscript 'bike' reminds us that the metric is defined for a motorcycle. 'p-p' indicates the peak-to-peak values, while 'avg' means 'average' throughout the manoeuvre. The index describes the steering torque required to obtain a unitary yaw rate response, normalised by the vehicle's speed. Using the peak-to-peak values instead of the absolute peak value, we capture a complete view of the manoeuvre entry [29], reducing the variation in metric values compared to indices using only the absolute peak, like the Koch Index [30], as shown by Cossalter [29]. This fact, along with the index being the ratio of the input τ and output $\dot{\psi}$, reduces the riding style influence on its value.

For the simplified car model, an equivalent metric must be defined: the steering input for the car is the kinematic steering angle instead of the steering torque, so we define the *Adapted* Lane Change Yaw Index (ALCYI) as:

$$\mathrm{ALCYI}_{\mathrm{car}} := \frac{\delta_{\mathrm{p\text{-}p}}}{\dot{\psi}_{\mathrm{p\text{-}p}} v_{\mathrm{avg}}}, \tag{8}$$

where we use the kinematic steering input δ instead of the steering torque. For the metrics to be comparable, the two must be dimensionally homogeneous. By multiplying the ALCYI by the absolute value of the Calibration gain, we obtain the following:

$$\mathrm{LCYI}_{\mathrm{car}} = |K_{\mathrm{steer}}|\mathrm{ALCYI}_{\mathrm{car}} = |K_{\mathrm{steer}}|\frac{\delta_{\mathrm{p\text{-}p}}}{\dot{\psi}_{\mathrm{p\text{-}p}} v_{\mathrm{avg}}}. \tag{9}$$

The simulator user would perceive manoeuvrability similar to the reference motorcycle during a lane change only if $\mathrm{LCYI}_{\mathrm{car}} \approx \mathrm{LCYI}_{\mathrm{bike}}$. So, the car parameters must be tuned to obtain this equivalence. For the single-track model, the yaw rate $\dot{\psi}$ is defined as the angular speed around the axis perpendicular to the ground; this is not the case for BikeSim© or most experimental data, where the yaw rate measured by the Inertial Measurement Unit is expressed in the tilting motorcycle frame. In such case, the measured yaw rate measured must be converted into the one relative to the vertical axis [19]:

$$\dot{\psi} = \frac{\dot{\psi}_{\mathrm{IMU}}}{\cos\phi}, \tag{10}$$

where ϕ is the roll angle.

The simplicity of the car model used allows calculating $\mathrm{LCYI}_{\mathrm{car}}$ analytically from its parameters, under some assumptions.

3.2.1 Manoeuvrability as a transfer function

The aim is to identify the transfer function that describes $\mathrm{LCYI_{car}}$ so that we can change the car parameters to make it equal to $\mathrm{LCYI_{bike}}$.

Equation (8) links the control input δ and the output $\dot{\psi}$: thus, it is necessary to express the transfer function describing the yaw rate response per unit of steering angle. The output equation joins the state Eq. (2):

$$\boldsymbol{y} = \mathrm{C}\boldsymbol{x} + \mathrm{D}\boldsymbol{u}, \tag{11}$$

where, in our specific case, $\boldsymbol{y} = \dot{\psi}$, $\boldsymbol{u} = \delta$ and consequently, using $\boldsymbol{x} = (\beta, \dot{\psi})^T$, we get $\mathrm{C} = [0, 1]$, $\mathrm{D} = 0$. For a continuous, time-invariant, linear state-space system, the transfer function $\mathrm{H}(s)$ between the Laplace transform of the input $\mathrm{U}(s)$ and output $\mathrm{Y}(s)$ can be calculated as:

$$\mathrm{H}(s) := \frac{\mathrm{Y}(s)}{\mathrm{U}(s)} = \mathrm{C}(s\mathrm{I} - \mathrm{A})^{-1}\mathrm{B} + \mathrm{D}, \tag{12}$$

where s is the Laplace variable, and I the identity matrix.

In our case, Eq. (12) provides the expression for the transfer function $\dot{\psi}(s)/\delta(s)$, which is the yaw rate output per unit of steering angle input for a specific complex frequency. So, we can divide the reciprocal of $\mathbf{H}(s)$ by the constant speed v to obtain the transfer function that describes the Adapted Lane Change Yaw Index:

$$\mathrm{ALCYI_{car}}(s) = \frac{1}{\mathrm{H}(s)v} = \frac{\delta(s)}{\dot{\psi}(s)v}. \tag{13}$$

$\mathrm{ALCYI_{car}}(s)$ consists of a static gain, two zeros and one pole. It is shown, for the understeering car parameters chosen in the quasi-static calibration, as a function of frequency in Fig. 6: its left limit is equal to

$$\lim_{\omega \to 0} \mathrm{ALCYI_{car}}(\omega) = \frac{l\left(1 + \eta v^2\right)}{v^2}, \tag{14}$$

which, as expected, coincides with Eq. (3) divided by $\dot{\psi}v$ (quasi-static behaviour). Compared to the static value, the $\mathrm{ALCYI_{car}}$ decreases for low-medium frequency inputs (better manoeuvrability, lower steering angle input required for a given yaw rate), reaching a minimum around 0.6 Hz. It increases monotonically for higher frequencies, with a unitary slope in the log–log plot, indicating a proportionality between the two quantities.

The linearised, single-track car model with understeering behaviour already describes the quasi-static manoeuvrability of the reference motorcycle. The next step is to tune the car parameters to obtain the desired transient manoeuvrability without

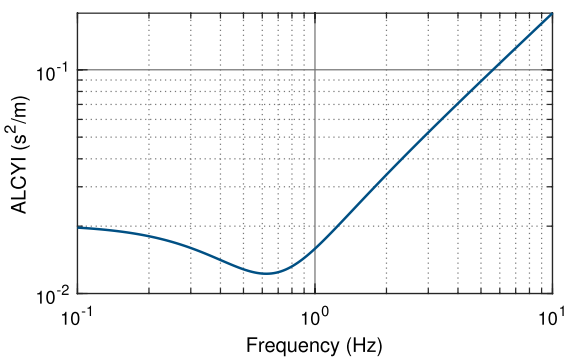

Fig. 6 Magnitude of the Adapted Lane Change Yaw Index calculated as a transfer function, as a function of the input frequency

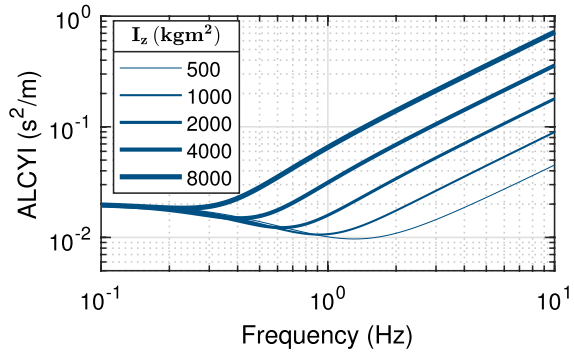

(a) Influence of the yaw inertia ($v = 80\,\mathrm{km\,h^{-1}}$)

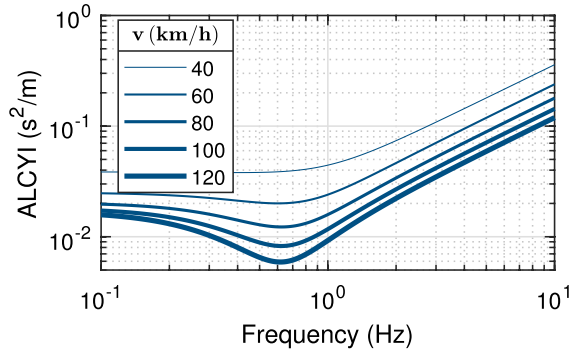

(b) Influence of the speed ($I_z = 2000\,\mathrm{kg\,m^2}$)

Fig. 7 Influence of car and manoeuvre parameters on the Adapted Lane Change Yaw Index. Thicker lines indicate higher parameter values. For each subfigure, the middle line corresponds to the previous figure

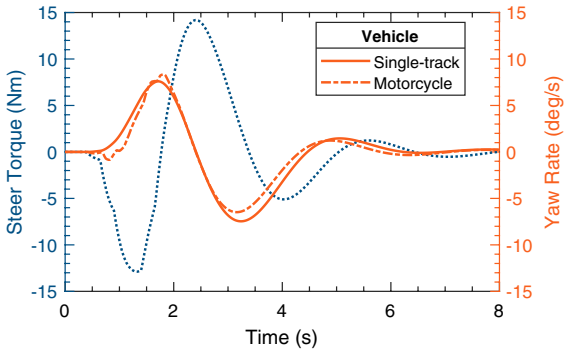

Fig. 8 Steering torque input (dotted blue line) and yaw rate outputs (solid and dash-dot orange line for the tuned single-track car model and reference motorcycle, respectively) during a left lane change manoeuvre (offset = 3 m, transition distance = 20 m, speed = 80 km h^{-1}). Counterclockwise torques and rotations are positive. (Color figure online)

affecting the quasi-static behaviour. As Eq. (4) shows, the only parameter that does not influence it is the yaw inertia I_z: by changing it, we can obtain the desired manoeuvrability in the typical input frequency range, without detrimental effects on the already tuned stationary behaviour.

Figure 7a shows the influence of the yaw inertia I_z on $\mathrm{ALCYI_{car}}$: increasing it lowers the frequency corresponding to the minimum magnitude, consequently reducing the maximum decrease of the chosen metric compared to the quasi-static value. As expected, the inertia does not influence the quasi-static value of the index. For sufficiently high values, it also affects the response to low-medium frequency inputs that constitute the bulk of the control action during a lane-change manoeuvre. The logarithmic spacing used for the yaw inertia values leads to equal vertical spacing of the transfer functions in the log–log plot in the mid to high-frequency range: in this range $\mathrm{ALCYI_{car}} \propto I_z$ (The yaw inertia dominates the transfer function).

Figure 7b considers, instead, the influence of speed v on $\mathrm{ALCYI_{car}}$: the influence is significant and is geometrically the same at low and high frequencies, with a more substantial effect at medium frequencies. We can describe its influence at lower frequencies by rewriting Eq. (14) as $\lim_{\omega\to 0} \mathrm{ALCYI_{car}}(\omega) = l\left(1/v^2 + \eta\right)$: the left limit linearly depends on $1/v^2$, so it tends to increase significantly when speed decreases starting from low values. Instead, η dominates the parentheses for higher speed values, and speed influence is reduced. This result provides a partial[3] analytical justification for the calibration speed influence on the error map (Fig. 5). However, the single-track model already considers this influence through the dependency of the system matrix A in Eq. (1).

Table 1 Comparison between the Lane Change Yaw Index of the reference motorcycle and the tuned single-track model for five different lane change tests

Test name	$\mathrm{LCYI_{bike}}$ (N rad^{-1} s^{-2})	$\mathrm{LCYI_{car}}$ (N rad^{-1} s^{-2})	Error (%)
3 m × 20 m, 80 km h^{-1}	**4.71**	**4.64**	**– 1.5**
3 m × 14 m, 80 km h^{-1}	5.65	5.72	1.2
3 m × 26 m, 80 km h^{-1}	4.56	4.23	– 7.2
3 m × 20 m, 60 km h^{-1}	3.36	5.60	66.5
3 m × 20 m, 100 km h^{-1}	5.99	3.80	– 36.7

The reference manoeuvre, used for the yaw inertia tuning, is in bold

If the frequency range of the input is known, it is possible to determine the I_z that equates the car and motorcycle transient manoeuvrability indexes, completing the equivalence.

3.2.2 *Yaw inertia tuning*

The aim is to determine the calibration yaw inertia I_z^* that satisfies $\mathrm{LCYI_{car}}|_{I_z^*} = |K_{\mathrm{steer}}|\mathrm{ALCYI_{car}}|_{I_z^*} \approx \mathrm{LCYI_{bike}}$, for a specific reference manoeuvre.

The chosen manoeuvre was a lane change with a 3 m offset and a 20 m transition distance, as used by Cossalter [29], with a target speed equal to the calibration speed $v^* = 80$ km h^{-1}. BikeSim© was employed to simulate motorcycle behaviour; in particular, the *Sports Small* model was used, as in Sect. 3.1. Due to the complex nature and rigorous tuning of its coefficients, the BikeSim© rider should provide a realistic input to the motorcycle. The motorcycle follows the input path using a feedforward controller considering lean angle and curvature control gains, and maximum lean angle and rate values. The controller was tuned according to the available literature and provided the instantaneous target lean to the speed-sensitive PID controller that calculated the appropriate steering

[3] The limit considers the influence of speed on the required car input, but no such influence on the required *motorcycle* input.

Table 2 Calibration gain K^*_{steer} and yaw inertia I^*_z for the three motorcycle models and each calibration speed

Motorcycle	v^* (km h^{-1})	K^*_{steer} (N m rad^{-1})	I^*_z (kg m^2)
Touring	60	− 81.9	36,000
	80	− 77.4	38,000
	100	− 73.5	40,000
Scooter	60	− 50.7	31,000
	80	− 60.3	26,000
	100	− 67.4	23,000
Sports small	60	− 72.8	15,000
	80	− 87.7	24,000
	100	− 98.0	34,000

Due to the small influence of the corner radius on the calibration gain, the reference corner radius is $R = 200$ m. The value of each coefficient can be interpolated between the three speed values, obtaining speed-dependent $K_{steer}(v)$ and $I_z(v)$. The other single-track, understeering car model properties do not change and are the following: $C_f = 21{,}000$ N rad^{-1}, $C_r = 39{,}000$ N rad^{-1}, $l_f = l_r = 1.5$ m, $m = 1300$ m

torque. . Moreover, due to the nature of the index adopted, the virtual rider characteristics should not be critical for assessing motorcycle manoeuvrability.

The measured input torque, yaw rate in the vertical direction, and speed were used to calculate $LCYI_{bike}$ through Eq. (7): the obtained reference value was 4.71 N rad^{-1} s^{-2}.

To tune the yaw inertia of the car, the steering angle input $\delta(t)$ was required; it was obtained by dividing the steering torque $\tau(t)$ applied by the motorcycle rider by the calibration gain K_{steer} (Eq. (6)). Next, we calculated the output $\dot{\psi}(t)$ of the single-track model subject to this input using the transfer function in Eq. (12):

$$\begin{aligned}\dot{\psi}(t) = y(t) &= \mathcal{L}^{-1}(\mathrm{Y}(s)) = \mathcal{L}^{-1}(\mathrm{H}(s)\mathrm{U}(s)) \\ &= \mathcal{L}^{-1}(\mathrm{H}(s)\mathcal{L}(\delta(t))),\end{aligned} \tag{15}$$

where $\mathcal{L}$ denotes the Laplace Transform. $\delta(t)$, $\dot{\psi}(t)$ and $v(t)$ signals were used to calculate $\delta_{p\text{-}p}(t)$, $\dot{\psi}_{p\text{-}p}(t)$ and $v_{avg}(t)$ that were employed to compute $ALCYI_{car}$ using Eq. (8). Lastly, $LCYI_{car}$ was calculated as $|K_{steer}|ALCYI_{car}$ (Eq. (9)).

H(s) depends on the yaw inertia I_z: consequently, $LCYI_{car}$ was calculated using the previous procedure for 100 yaw inertia values, equally spaced between 1000 kg m^2 and 100,000 kg m^2. $LCYI_{car}$ monotonically increased with I_z and did so linearly for mid to high yaw inertia values[4]. The yaw inertia value that resulted in a Lane Change Yaw Index equal to the reference motorcycle was $I^*_z = 24{,}000$ kg m^2. This value is unrealistically high for a car, but it is the one that should provide similar manoeuvrability to the reference motorcycle.

By definition, this yaw inertia value provided equal LCYI. Moreover, the input signal (the steering torque τ) was the same for motorcycle and car, for which it was scaled (and its sign changed) by the calibration gain K_{steer}: consequently, this translated

(a) Overview, showing the tilting mockup

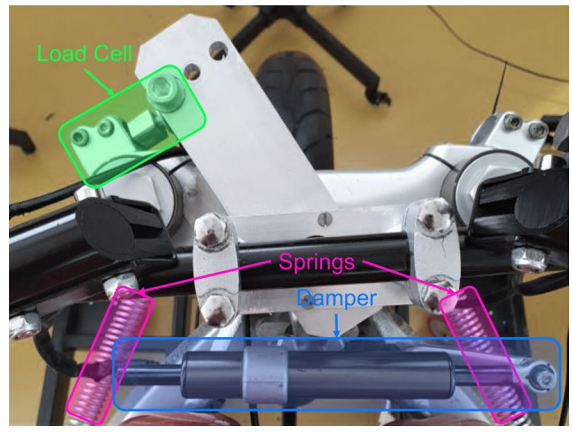

(b) Detail of the steering assembly

Fig. 9 Architecture of the simulator used

[4] This is coherent with what has been discussed in Sect. 3.2.1 about Fig. 7a: in fact, the influence of I_z on $LCYI_{car}$ can be thought of as a section of Fig. 7a for a certain frequency or, more exactly, the frequency interval corresponding to the steering input.

into having the same $\ddot{\psi}_{\text{p-p}}$. However, it is essential to check whether the car and motorcycle yaw rates show similar shape, phase and frequency. Figure 8 directly compares the time signals (counterclockwise torques and rotations are positive) during the left Lane Change: although the peak-to-peak yaw rate values are the same, some differences emerge. The motorcycle response was more erratic for the same input due to its more complex and nonlinear nature. In particular, although both vehicles counter-steered, in the very first part of the manoeuvre, the motorcycle yaw rate had the same sign as the steering torque due to the bike having to initially steer to the right for the centrifugal force to make it lean to the left [29]. Due to its nature, the tuned car model could not reproduce this behaviour. Lastly, the time interval between the two yaw rate peaks was slightly different, amounting to 1.52 s and 1.33 s for the car and motorcycle models, respectively. These results are positive and confirm the potential of the approach. Alternatively, the yaw inertia was tuned to have the same peak-to-peak yaw *acceleration* $\dddot{\psi}_{\text{p-p}}$, with similar results in terms of inertia. Appendix C expands this discussion.

Lastly, we checked for the robustness of the approach to different lane change parameters. In particular, the BikeSim© simulation was repeated with different transition distances (14 m and 26 m, instead of the default 20 m) and speeds (60 km h^{-1} and 100 km h^{-1}, instead of the default 80 km h^{-1}). In terms of LCYI, results are summarised in Table 1: a significant change in the transition distance did not increase the error significantly, and the car model correctly predicted the change in the metric due to the different manoeuvre geometry. The rider's steering torque frequency content was not significantly affected by the manoeuvre geometry, so the transfer function, with I_z^* determined through the reference manoeuvre, was evaluated in a similar frequency range, resulting in a moderate error. In contrast, a significant variation in the manoeuvre speed led to appreciable error, especially if it was reduced. The LCYI values from the BikeSim© model were coherent with those found by Cossalter [29] for a similar motorcycle. Further analysis of the influence of these lane change parameters along with the signals plots is provided in Appendix D.

A single value for K_{steer}^* and I_z^* is therefore sufficient to reproduce both quasi-static and transient manoeuvres at a certain speed, with different cornering radii and geometries. Table 2 provides the K_{steer}^*, I_z^* values for each motorcycle model and each speed. These values can make the single-track model manoeuvrability analogous to the reference motorcycle, both in quasi-static and transient conditions. Moreover, the value of each coefficient can be interpolated between the three speed values, obtaining speed-dependent $K_{\text{steer}}(v)$ and $I_z(v)$. The other parameters of the understeering single-track model do not vary, and are the following: $C_{\text{f}} = 21{,}000\,\text{N rad}^{-1}$, $C_{\text{r}} = 39{,}000\,\text{N rad}^{-1}$, $l_{\text{f}} = l_{\text{r}} = 1.5\,\text{m}$, $m = 1300\,\text{m}$.

4 Objective validation on the simulator

In this section, the calibrated single-track car is used as the dynamic model of a simulator to objectively validate the approach. The vehicle response to the rider steering torque is investigated and compared to BikeSim© simulations of the same manoeuvres, using the reference motorcycle.

4.1 Apparatus and methods

Figure 9 illustrates the simulator used, which was an evolution of that described by Savino [10]. The motorcycle mockup consisted of a small sports motorcycle with the engine and rear swingarm removed, connected to a fixed base through a rotational joint allowing passive tilting (Fig. 9a). Figure 9b shows the steering assembly. Helical springs connected it to the motorcycle frame, providing a restoring torque that produced the steering torque feedback. The vehicle's standard steering damper was present, creating a damping effect. A load cell measured the steering torque applied by the rider.[5] The stiffness of the helical springs determined the proportionality between the applied steering torque and the resulting steering angle of the mockup; however, this did not influence the simulation: in fact, the input to the simulation was the measured steering torque, that was converted into a car steering angle through the gain K_{steer}. The rotation of the front assembly of the mockup was only used to increase the perceived realism: the stiffness of the springs provided a ratio between applied torque

[5] By directly measuring the torque, it was possible to measure the transient torques applied by the rider that would be missed by measuring the steering rotation and converting it to a steering torque via the known torsional stiffness.

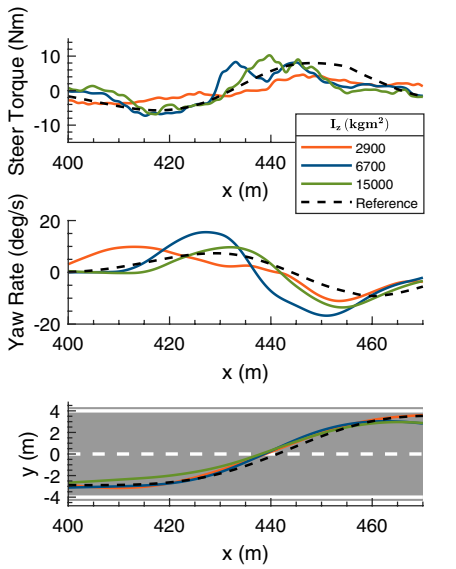

(a) Lane change (30 m transition distance)

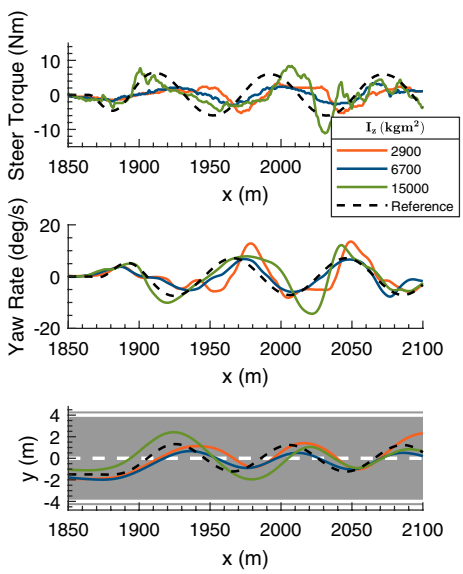

(b) Slalom (40 m spacing)

Fig. 10 Steering torque (top), yaw rate (middle) and lateral position (bottom) as a function of the longitudinal position for two different 60 km h^{-1} manoeuvres. The solid, coloured lines indicate the single-track model used in the simulator, with three different yaw inertia values. The dashed, black line refers to the reference motorcycle. (Color figure online)

and steering angle corresponding to a real motorcycle and allowed reaching the maximum torques required within the limited rotation permitted by the handlebar. Peculiarly, given the counter-steering input

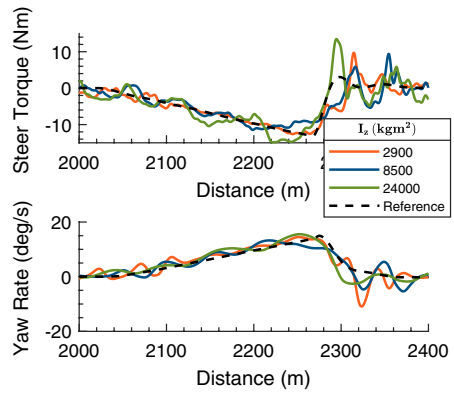

(a) Decreasing radius corner ($R_{\min} = 80$ m)

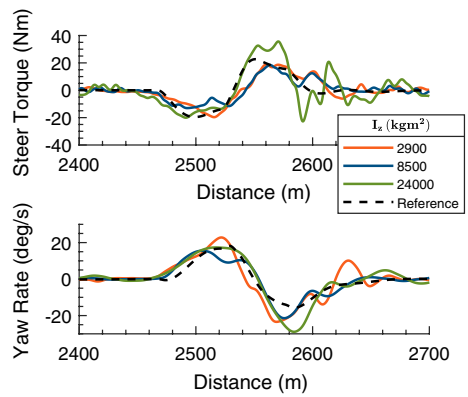

(b) Chicane ($R = 70$ m)

Fig. 11 Steering torque (top) and yaw rate (bottom) as a function of the travelled distance for two different 80 km h^{-1} manoeuvres. The solid, coloured lines indicate the single-track model used in the simulator, with three different yaw inertia values. The dashed, black lines refer to the reference motorcycle. (Color figure online)

torque exerted by the rider and the elastic relationship between it and the resulting steering angle, the steering assembly rotates towards the *outside* of the corner, contrary to what happens in a real motorcycle in most driving conditions.[6] A throttle grip rotation sensor and pressure sensors on the two channels of the braking system allowed speed control. A microcontroller-based system (Arduino Leonardo) transferred the inputs from the sensors to a personal computer.

Simcenter Prescan© was used to create the riding scenarios; the software allowed car dynamics

[6] The rotations are small and with low angular velocities, so this physical inconsistency is not noticeably perceived.

Table 3 Lane Change Yaw Index (N rad^{-1} s^{-2}) calculated for the six different transient manoeuvres, for three Yaw Inertia values for the single-track model used in the simulator and the reference motorcycle

For the slalom manoeuvre, the index was calculated as the average of the three indexes obtained with the three couples of peaks. The average for all the manoeuvres at the same speed is indicated in bold

Manoeuvre		Vehicle LCYI			
Geometry	Speed (km h^{-1})	Low-inertia (N rad^{-1} s^{-2})	Mid-inertia (N rad^{-1} s^{-2})	High-inertia (N rad^{-1} s^{-2})	Reference (N rad^{-1} s^{-2})
Lane Change 30 m	60	1.34	1.58	2.74	2.86
Lane Change 26 m	60	1.49	1.46	2.21	2.88
Lane Change 22 m	60	1.49	1.39	1.95	2.97
Lane Change 18 m	60	1.42	1.46	2.82	3.14
Slalom 40 m	60	1.35	1.46	2.62	2.91
Chicane $R = 70$ m	80	2.12	2.25	3.20	3.22
Average	**60**	**1.42**	**1.47**	**2.47**	**2.95**
Average	**80**	**2.12**	**2.25**	**3.20**	**3.22**

Table 4 Delay (s) between the input Steering Torque and output Yaw Rate calculated for ten different manoeuvres, for three Yaw Inertia values for the single-track model used in the simulator and for the reference motorcycle

The delay was estimated by maximising the cross-correlation between the two signals. The average for all the manoeuvres at the same speed is indicated in bold

Manoeuvre		Vehicle delay			
Geometry	Speed (km h^{-1})	Low-inertia (s)	Mid-inertia (s)	High-inertia (s)	Reference (s)
Lane change 30 m	60	0.25	0.50	0.77	0.75
Lane change 26 m	60	0.34	0.52	0.75	0.70
Lane change 22 m	60	0.35	0.52	0.75	0.70
Lane change 18 m	60	0.34	0.52	0.73	0.70
Slalom 40 m	60	0.33	0.49	0.74	0.78
Corner $R = 300$ m	80	0.33	0.53	0.97	1.00
Corner $R = 200$ m	80	0.33	0.57	0.98	0.95
Corner $R = 100$ m	80	0.29	0.53	0.88	0.90
Clothoid $R_{min} = 80$ m	80	0.34	0.57	0.90	0.85
Chicane $R = 70$ m	80	0.28	0.53	0.93	0.88
Average	**60**	**0.32**	**0.51**	**0.75**	**0.73**
Average	**80**	**0.31**	**0.55**	**0.93**	**0.92**

simulation through models of differing complexity. The simplified model was chosen, consisting of a linearised, single-track model as that described in this article.

Two scenarios were used in the experiment:

- A two-lane straight road with a 60 km h^{-1} speed limit, with cones used to create deviations from the right lane. The scenario included four lane changes with progressively lower transition distances, to become more severe the more experience the rider gathered, and a final slalom manoeuvre.
- A three-lane country road with an 80 km h^{-1} speed limit, consisting of corners connected by straight sections. The corners were progressively more severe: three constant radius bends, with radii 300 m, 200 m, 100 m, respectively, were followed by a decreasing radius corner, consisting of a clothoid with a final radius of 80 m. The scenario concluded with a fast chicane with two 70 m radius corners.

The car model had parameters taken from Table 2, relative to the *Sports Small* motorcycle model. K^*_{steer} and I^*_z were the ones relative to the recommended scenario speed. For comparison, two other I_z values were used:

- A value relative to a car with equal mass and wheelbase to the single-track model parameters, equal to 2900 kg m^2 [31, Eq. 18a].

- An intermediate value between the one obtained through calibration and the one estimated for a car of equal parameters. As Fig. 7a showed a logarithmic influence of the inertia on manoeuvrability, the geometric mean between the two values was chosen.

The course was then repeated through BikeSim© using the reference *Sports Small* model: the simulation signals served as the reference values.

One of the authors performed the virtual riding: the scope of this validation was to verify whether the approach, developed and calibrated analytically and through computer simulations, produced the desired results when implemented on the simulator with a rider in the loop. Therefore, the validation was quantitative and objective: a subjective validation had been performed [10] for the simulator from which this one descends, with good feedback regarding the steering feel. Compared to that, the hardware was upgraded, and the car model was calibrated with the proposed approach.

4.2 Test results

In this subsection, the input (the measured steering torque) and output (the yaw rate and coordinates of the virtual vehicle) simulator signals are compared to those of the BikeSim© simulation. A global, succinct description of the dynamics is provided in tables for each manoeuvre, while a representative subset is investigated in detail through the signals plots.

Figure 10 shows the steering torque, yaw rate and coordinates during each trial, with three different colours for the three yaw inertia values used, for two manoeuvres of the 60 km h^{-1} course. The dashed, black line represents the simulation using the reference motorcycle. In particular, Fig. 10a shows the first lane change encountered, with a 30 m transition distance and approximately 4 m offset. As expected, the higher the yaw inertia, the higher the peak-to-peak steering torque the rider applies. Despite its higher input, the high-inertia model showed a smaller yaw rate response than the mid-inertia model. The lower response of the low-inertia model than the mid-inertia one is justified by the input torque being significantly smaller: this reflects on the more open trajectory compared to the mid-inertia model. Although the single signals were influenced by how the rider approached the manoeuvre, this should have limited influence on the input–output response, as shown by Cossalter [29] for real motorcycles and later in this section for the simulator data. Figure 10b shows the same quantities for the slalom manoeuvre, with similar results.

Figure 11 shows the steering torque and yaw rate relative to two manoeuvres of the 80 km h^{-1} course. The decreasing radius corner (Fig. 11a) has both steering torque and yaw rate increasing throughout the manoeuvre and having opposite signs due to counter-steer. All the runs followed the reference data, with no evident influence of the yaw inertia. Lastly, Fig. 11b shows the signals for the demanding fast chicane: as expected, the model with the highest yaw inertia required the highest steering torque.

Table 3 shows the Lane Change Yaw Index values for all the transient manoeuvres of the two courses, for the three different yaw inertia values and for the reference motorcycle. For a motorcycle, the index tends to increase with speed, as shown by Cossalter [29] and by the average value for each speed in Table 1. Comparing the manoeuvres at 60 km h^{-1}, the index value tended not to change with the manoeuvre for both the single-track and motorcycle models. Instead, there was a significant influence of the yaw inertia: the low-inertia and mid-inertia models showed a much lower value than the reference motorcycle, while the high-inertia one was much closer to the desired value. This observation carried on to the 80 km h^{-1} chicane.

Table 4 shows the input–output delay[7] for all the manoeuvres. There was a monotone relationship between the car inertia and the input–output delay; the high-inertia model matched the delay of the reference motorcycle. Moreover, the reference delay showed an approximately proportional relationship with speed; the high-inertia model showed the same trend, while the lower-inertia models did not display significant variation. The average value for all the manoeuvres at each speed clearly shows this evidence.

5 Discussion

Results showed a good agreement between the calibrated single-track model and the reference motorcycle, confirming the similar quasi-static and transient manoeuvrability already verified analytically and in simulation in Sect. 3.

[7] The delay was obtained by maximising the cross-correlation between the two signals.

Regarding quasi-static behaviour and manoeuvrability, results for the decreasing radius corner (Fig. 11a) showed that the tuned car model responded to a quasi-static steering torque increase similarly to the motorcycle. The corner covers all the radii down to 80 m; on the other hand, K^*_{steer} is constant and relative to a 200 m radius corner: this confirms that the influence of corner radius on the calibration gain is tiny and that the model can describe corners of widely different radii with a single calibration point. This result is coherent with the almost horizontal contour lines of Fig. 4. As expected, car behaviour was not influenced by its yaw inertia during quasi-static manoeuvres. Interestingly, in the realignment phase, both the car and motorcycle models showed an overshoot in the steering torque input, which was briefly directed towards the *inside* of the corner.

The manoeuvrability agreement extended to the transient manoeuvres. The amplitude and phase of the input–output relationship were described by the LCYI and delay values, respectively (Tables 3, 4). The car model with calibrated inertia showed index values coherent with the reference motorcycle, independently of the manoeuvre type or speed, validating the calibration approach. Although the aim was to equal the *amplitude* of the yaw rate response of the motorcycle, the *phase* of the response was also correctly reproduced. The reason is that the transfer function *gain* was set through quasi-static manoeuvres, while the correct amplitude of the transient response was obtained by changing only the yaw inertia of the car. This fact translated into reproducing both the static and transient amplitude response, linked to having similar transfer functions, which implies similar phase responses.

There was an appreciable difference in the response delay of the different models: the Lane Change Yaw Index showed close results between the low and mid-inertia models, while the high-inertia model took on distinct values close to the reference motorcycle. Figure 7a justifies this: for low enough I_z values, the response amplitude is not influenced by the inertia up to frequencies above the steering input.

The rider noticed that the vehicle tended to slide laterally when performing the most demanding manoeuvres using the high-inertia model. This phenomenon occurred because, in order to have similar manoeuvrability to the motorcycle, the car required a yaw inertia value much higher than a conventional car with similar cornering stiffness. This study considered the steering torque to yaw rate response, while the other state (the vehicle slip angle β) was only used as an intermediate state that linked the input to the other state because the yaw motion is the most evident motion of the vehicle and it dominates its trajectory control. However, the slip angle can be explicitly neglected only if its value remains small: for the high-inertia model, it reached 5° during the 18 m lane change and 8° during the demanding chicane manoeuvre. While noticeable, the rider could always keep the vehicle in the desired lane, as shown for two other manoeuvres in Fig. 10, showing good trajectory repeatability despite different inertia values. The consequences on the perceived realism have not been investigated: future work could observe the influence of the yaw inertia on the steering torque to slip angle transfer function and evaluate these aspects with external participants.

We conclude that the experimental test validated the proposed approach as a reproducible, clear and unambiguous way to describe motorcycle manoeuvrability through a tuned single-track model. The input–output relationship chosen was correctly reproduced for both quasi-static and transient manoeuvres, for different speeds and radii, in both amplitude and phase.

Expanding from the validation test to the whole approach, a common pattern has been found between the motorcycle steering torque and the steering angle of an understeering car required to corner with a given radius and speed. The ratio of the two inputs, negative due to the motorcycle counter-steer, can be used as a gain to make the car respond to a steering torque input similarly to a motorcycle, with reasonable error in a broad radius-speed region. This gain was employed to compare car and motorcycle transient manoeuvrability. It allowed the definition of the transfer function describing car manoeuvrability as a function of frequency, with a known influence of yaw inertia and speed. This transfer function was used to tune the car yaw inertia using the steering torque exerted on a high-fidelity motorcycle model during a simulated lane change manoeuvre to have the same peak-to-peak response. The robustness of the approach was verified by changing the manoeuvre parameters.

Future development could consist of interpolating the calibration gain and yaw inertia values provided in Table 2 and testing the accuracy in reproducing manoeuvres at intermediate speeds. The approach is promising, and this work facilitates the realisation of simplified motorcycle simulators capable of

reproducing the response of various motorcycle classes. As a next step, a test with volunteers could rate the subjective simulator realism in detail. The simpler the simulator, the lower the familiarisation time required [6]: the adaptation period length for this simulator could be compared to that of simulators of differing complexity. Moreover, it would be interesting to test whether participants can identify distinct motorcycles corresponding to different parameters. Lastly, in this work, the rider was focused and aware of the manoeuvres to be performed: the response in the presence of unexpected obstacles or distractions could be tested.

6 Conclusion

This article showed the similarity and differences between car and motorcycle manoeuvrability, the car parameters influencing it and how they can be tuned to reproduce the response of different motorcycles, in terms of both amplitude and phase. These results were used to build a motorcycle simulator based on a linear, single-track car model, with a positive outcome. Additional advantages are the stability and availability of such a simple dynamic model and its reduced computational burden, lowering hardware requirements.

This work allows the development of low-complexity and cost-effective simulators with good fidelity properties. The resulting car parameters, relative to different motorcycle classes and speeds, are provided and can be directly used in a simulator. The reduced number of parameters allows simple tuning. Furthermore, the low computational cost of the linearised single-track model makes it a candidate as the dynamic model for rider assistance systems and safety devices. In particular, the present work may pave the way to LPV gain scheduling techniques for motorcycle control. Lastly, it may allow converting a car simulator into a motorcycle simulator with realistic steering sensation by adding a low-complexity motorcycle mockup.

Acknowledgements The authors would like to thank Eng. Andrea Biffoli for his support and technical assistance with developing the MOVING simulator.

Funding Open access funding provided by Università degli Studi di Firenze within the CRUI-CARE Agreement. This research is part of the MASMOT project ('MAtematica per la Sicurezza dei MOTocicli' [MAthematics for MOTorcycle Safety]), which received funding from the Ente Cassa di Risparmio di Firenze https://www.fondazionecrfirenze.it/en/.

Availability of data and materials The data supporting the findings of this study are available from the corresponding author, Bartolozzi M, upon reasonable request.

Declarations

Conflict of interest The authors have no competing interests to declare that are relevant to the content of this article.

Appendix A: Additional details about the quasi-static simulations

For each vehicle, pseudo-stationary riding conditions were reproduced in the $[30\,\mathrm{km\,h^{-1}}, 130\,\mathrm{km\,h^{-1}}]$ speed range ($[8.3\,\mathrm{m\,s^{-1}}, 36.1\,\mathrm{m\,s^{-1}}]$) and turning radii $R > 20\,\mathrm{m}$. PI and PID controllers tracked the target speed and roll profiles, respectively. Speed increased with a longitudinal acceleration of $0.01\,\mathrm{m/s^2}$ to avoid an influence of longitudinal dynamics on lateral dynamics due to load transfer and combined slip. Simultaneously, a sinusoidal roll angle profile was imposed with a 40° amplitude and 200 s period: the low frequency excluded transient phenomena. A single simulation allowed continuous coverage of the speed and radius domain of interest. The period of the sine comprising the roll target, albeit extensive, was much smaller than the transition time from $30\,\mathrm{km\,h^{-1}}$ to $130\,\mathrm{km\,h^{-1}}$: so, after a period, the whole lateral acceleration range was spanned with a minor change in longitudinal speed. The PID controller applied the steering torque needed to follow the roll input.

Appendix B: Steering gain and error maps for the other motorcycle classes

Figure 12 shows the calibration gain maps considering the Touring and Scooter motorcycle models. The error maps relative to the same models are shown in Figs. 13 and 14.

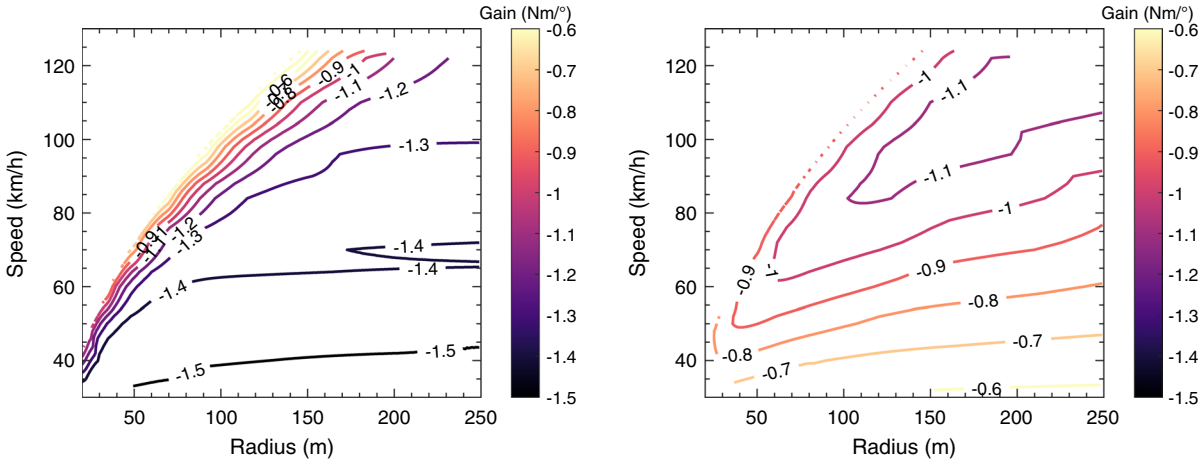

(a) Touring **(b)** Scooter

Fig. 12 Calibration gain maps for the other two motorcycle models

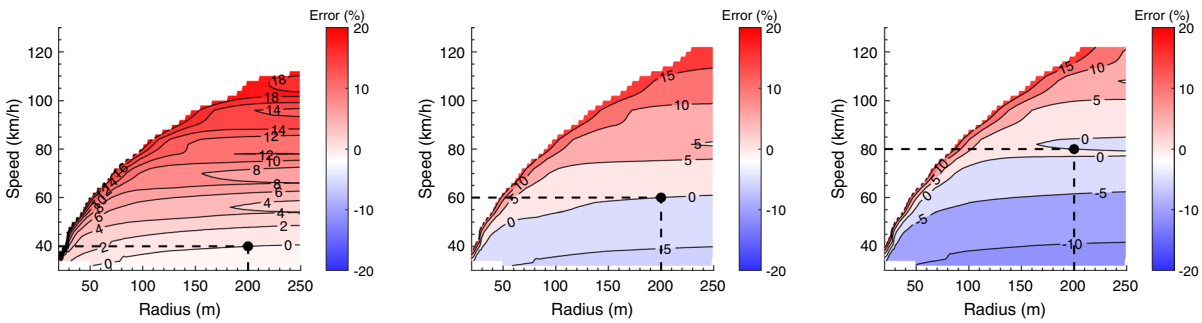

(a) $R^* = 200\,\mathrm{m},\ v^* = 40\,\mathrm{km\,h^{-1}}$ **(b)** $R^* = 200\,\mathrm{m},\ v^* = 60\,\mathrm{km\,h^{-1}}$ **(c)** $R^* = 200\,\mathrm{m},\ v^* = 80\,\mathrm{km\,h^{-1}}$

Fig. 13 Error maps for the *Touring* model

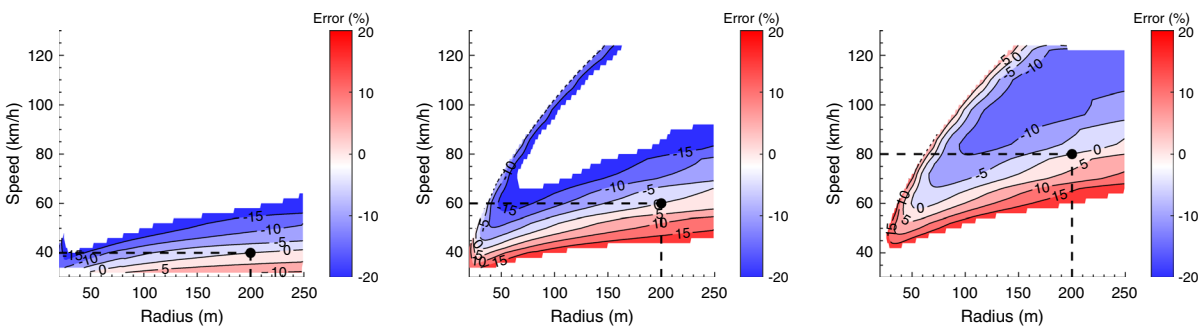

(a) $R^* = 200\,\mathrm{m},\ v^* = 40\,\mathrm{km\,h^{-1}}$ **(b)** $R^* = 200\,\mathrm{m},\ v^* = 60\,\mathrm{km\,h^{-1}}$ **(c)** $R^* = 200\,\mathrm{m},\ v^* = 80\,\mathrm{km\,h^{-1}}$

Fig. 14 Error maps for the *Scooter* model

Appendix C: Yaw inertia tuning considering yaw acceleration

As an alternative approach, the yaw inertia was tuned so that the two vehicles would have the same peak-to-peak yaw *acceleration* $\ddot{\psi}_{\text{p-p}}$ instead of yaw *rate* $\dot{\psi}_{\text{p-p}}$. The yaw inertia values were close (slightly lower) to those equalling the yaw rates. Consequently, we checked that the yaw inertia value tuned by equalling the first derivative also provided a value of the second derivative close to the reference value and vice versa. This result is linked to the oscillation period of the single-track model yaw rate being close to that of the motorcycle. Therefore, the approach of equalling the yaw rates has been chosen, as the two methods are almost equivalent.

Appendix D: Influence of lane change parameters

Figure 15 shows the influence of the variation of the manoeuvre parameters on the input torque of the rider and the output yaw rates of the single-track car model and reference motorcycle.

Figure 15a, b show the influence of the transition distance: its diminution makes the manoeuvre more demanding, requiring higher steering torque peaks to lean the motorcycle more quickly and increasing the amplitude of the initial yaw rate towards the outside of the corner. Changing the manoeuvre geometry compared to that used for the calibration does not make the agreement between the two models significantly worse.

Figures 15a, b show the influence of the speed: similarly to reducing the transition distance, an increase of the speed makes the manoeuvre harder, requiring higher input torques. Changing the speed compared to that used for calibration leads to an error in the yaw rate magnitude, albeit no worsening of the phase is noticed. It is to be noticed that, although Fig. 7b showed a significant influence of the speed on car behaviour, its effect is correctly taken into account through the dependency of the system matrix A in Eq. (1). Instead, the error is due to the different influence of v on $\text{LCYI}_{\text{bike}}$ and LCYI_{car}. The former shows an approximately proportional dependency on the speed, as shown by Cossalter [29];. At the same time, the latter, in the absence of a speed-variable calibration gain $K_{\text{steer}}(v)$, tends to decrease with speed, as shown in terms of *Adapted* Lane Change Yaw Index by Fig. 7b. Using a speed-variable calibration gain, the error at speeds different from

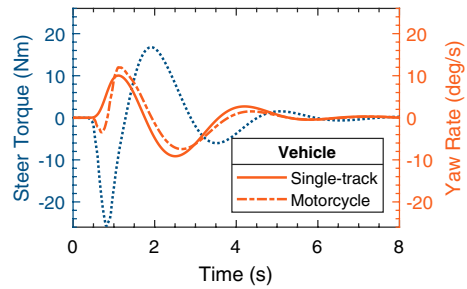

(a) Reduced transition distance (14 m)

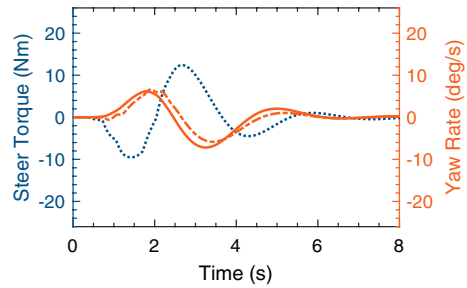

(b) Increased transition distance (26 m)

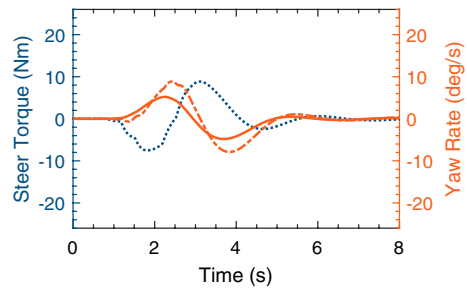

(c) Reduced speed (60 km h^{-1})

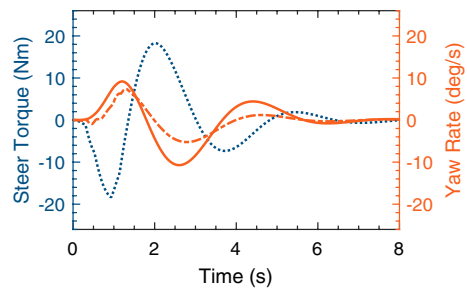

(d) Increased speed (100 km h^{-1})

Fig. 15 Comparison between single-track model (solid, orange line) and reference motorcycle (dash-dot, orange line) yaw rates for transition distances and speeds different to those of the calibration manoeuvre (20 m, 80 km h^{-1}). (Color figure online)

the calibration one would decrease: as shown by Fig. 4, an increase in speed would increase the gain, making $LCYI_{car}$ increase due to Eq. (9). Additionally, speed-dependent yaw inertia $I_z(v)$ would further reduce the error. So, the solution to make the influence of speed on the transient manoeuvrability similar to its influence on that of the motorcycle would be to tune the yaw inertia for different speeds and use adaptive inertia $I_z(v)$ with a law obtained through regression of the single values, joined by a speed-dependent gain $K_{steer}(v)$.

References

1. Cossalter V, Lot R, Massaro M, Sartori R (2011) Development and validation of an advanced motorcycle riding simulator. Proc Inst Mech Eng Part D J Automob Eng 225(6):705–720. https://doi.org/10.1016/s0389-4304(01)00147-3
2. Cossalter V, Lot R, Massaro M (2010) An advanced multibody code for handling and stability analysis of motorcycles. Meccanica 10(46):943–958. https://doi.org/10.1007/s11012-010-9351-7
3. Cossalter V, Lot R, Rota S (2010) Objective and subjective evaluation of an advanced motorcycle riding simulator. Eur Transp Res Rev 12(2):223–233. https://doi.org/10.1007/s12544-010-0041-2
4. Arioui H, Nehaoua L, Hima S, Séguy N, Espié S (2010) Mechatronics, design, and modeling of a motorcycle riding simulator. IEEE/ASME Trans Mechatron 15(5):805–818. https://doi.org/10.1109/tmech.2009.2035499
5. Massaro M, Cossalter V, Lot R, Rota S, Ferrari M, Sartori R et al (2013) A portable driving simulator for single-track vehicles. In: IEEE International conference on mechatronics (ICM), vol 2013, pp 364–369. https://doi.org/10.1109/icmech.2013.6518564
6. Benedetto S, Lobjois R, Faure V, Dang NT, Pedrotti M, Caro S (2014) A comparison of immersive and interactive motorcycle simulator configurations. Transportation Res Part F Traffic Psychol Behav 23:88–100. https://doi.org/10.1016/j.trf.2013.12.020
7. Sahami S, Sayed T (2013) How drivers adapt to drive in driving simulator, and what is the impact of practice scenario on the research? Transport Res F: Traffic Psychol Behav 16:41–52. https://doi.org/10.1016/j.trf.2012.08.003
8. Stedmon AW, Brickell E, Hancox M, Noble J, Rice D (2012) MotorcycleSim: a user-centred approach in developing a simulator for motorcycle ergonomics and rider human factors research. Adv Transp Stud Int J 06(A-27):31–48. https://doi.org/10.4399/97888548486723
9. Lenkeit J (1995) A servo rider for the automatic and remote path control of a motorcycle. SAE Trans 104:367–372. https://doi.org/10.4271/950199
10. Savino G, Pierini M, Lenné MG (2016) Development of a low-cost motorcycle riding simulator for emergency scenarios involving swerving. Proc Inst Mech Eng Part D J Automob Eng 230:1891–1903. https://doi.org/10.1177/0954407015624998
11. Nugent M, Savino G, Mulvihill C, Lenné M, Fitzharris M (2019) Evaluating rider steering responses to an unexpected collision hazard using a motorcycle riding simulator. Transp Res F Traffic Psychol Behav 66:292–309. https://doi.org/10.1016/j.trf.2019.09.005
12. Cossalter V, Lot R (2002) A motorcycle multi-body model for real time simulations based on the natural coordinates approach. Veh Syst Dyn 37:423–447. https://doi.org/10.1076/vesd.37.6.423.3523
13. Mechanical Simulation Corporation.: BikeSim [Internet]. Cited Dec 21. Available from: https://www.carsim.com/products/bikesim/
14. Sharp RS, Evangelou SA, Limebeer DJN (2004) Advances in the modelling of motorcycle dynamics. Multibody Syst Dyn 12:251–283. https://doi.org/10.1023/b:mubo.0000049195.60868.a2
15. Sharp RS, Evangelou S, Limebeer DJN (2005) Multibody aspects of motorcycle modelling with special reference to autosim. Comput Methods Appl Sci 2:45–68. https://doi.org/10.1007/1-4020-3393-1_3
16. Besselink IJM, Schmeitz AJC, Pacejka HB (2010) An improved Magic Formula/Swift tyre model that can handle inflation pressure changes. Veh Syst Dyn 48(sup1):337–352. https://doi.org/10.1080/00423111003748088
17. Sharp RS (1971) The stability and control of motorcycles. Arch J Mech Eng Sci 1959–1982 (vols 1–23) 13:316–329. https://doi.org/10.1076/vesd.35.4.291.2042
18. Cossalter V (2006) Motorcycle dynamics. 2nd ed. Lulu.com
19. Bartolozzi M, Savino G, Pierini M (2021) Novel high-fidelity tyre model for motorcycles to be characterised by quasi-static manoeuvres—rationale and numerical validation. Veh Syst Dyn 1–27. https://doi.org/10.1080/00423114.2021.2013506
20. Cossalter V, Lot R, Massaro M, Peretto M (2011) Investigation of motorcycle steering torque components. In: AIP Conference proceedings, vol 1394, pp 35–46. https://doi.org/10.1063/1.3649934
21. Rucco A, Notarstefano G, Hauser J (2010) Dynamics exploration of a single-track rigid car model with load transfer. In: 49th IEEE conference on decision and control (CDC), pp 4934–4939
22. Isermann R (2021) Automotive control: modeling and control of vehicles, 1st edn. Springer, Berlin
23. Sierra C, Tseng E, Jain A, Peng H (2006) Cornering stiffness estimation based on vehicle lateral dynamics. Veh Syst Dyn 44(sup1):24–38. https://doi.org/10.1080/00423110600867259
24. Lugo L, Bartolozzi M, Vandermeulen W, Geluk T, Dom S (2021) Test-driven full vehicle modelling for ADAS algorithm development. In: Symposium on international automotive technology. SAE International
25. Cossalter V, Lio MD, Lot R, Fabbri L (1999) A general method for the evaluation of vehicle manoeuvrability with special emphasis on motorcycles. Veh Syst Dyn 31(2):113–135. https://doi.org/10.1076/vesd.31.2.113.2094
26. Cossalter V, Doria A, Lot R (1999) Steady turning of two-wheeled vehicles. Veh Syst Dyn 31(3):157–181. https://doi.org/10.1076/vesd.31.3.157.2013

27. Pacejka HB (2005) Tire and vehicle dynamics, 2nd edn. Butterworth-Heinemann
28. Higuchi A, Pacejka HB (1997) The relaxation length concept at large wheel slip and camber. Veh Syst Dyn 27(sup001):50–64. https://doi.org/10.1080/00423119708969644
29. Cossalter V, Sadauckas J (2006) Elaboration and quantitative assessment of manoeuvrability for motorcycle lane change. Veh Syst Dyn 44(12):903–920. https://doi.org/10.1080/00423110600742072
30. Koch J (1980) Experimentelle und analytische Untersuchungen des Motorrad-Fahrer-systems. VDI-Z 08:122
31. Fundowicz P, Sar H (2018) Estimation of mass moments of inertia of automobile. In: 2018 XI international science-technical conference automotive safety, pp 1–6